Hole-to-hole variations in coupled flow and spray simulation of a double-layer multi-holes diesel nozzle

Chuqiao Wang[1,2], Moro Adams[3], Tong Luo[1], Tianyu Jin[1], Fuqiang Luo[1,*], Manolis Gavaises[2]

(1. School of Automotive and Traffic Engineering, Jiangsu University, Zhenjiang, China;
2. School of Mathematics, Computer Science and Engineering, City, University of London, London, UK;
3. Faculty of Mechanical Engineering, Accra Technical University, Accra, Ghana)

Abstract

In direct injection diesel engines, double-layer multi-holes nozzles contribute significantly in making spray injection uniform in both the circumferential and axial directions; they further ensure that minimal or no interactions are encountered among the spray jets emerging from the nozzle holes and positively affect fuel atomization and enhance mixing during engine operation. In this study, the variation in internal flow characteristics and the subsequent spray patterns from the upper and the lower layer nozzle holes were investigated experimentally and computationally. A double-layer 8-hole heavy-duty diesel engine injector nozzle was utilised for the characterization of hole-to-hole variation on spray formation. The actual nozzle geometry was derived from X-ray scans obtained at the third generation X-ray imaging and biomedical beamline station in SSRF, revealing all geometrical differences between the individual injection holes. The momentum fluxes from each of the injection holes were obtained together with spray tip penetration under non-evaporating conditions. These data were used to validate the computational fluid dynamics (CFD) model suitable to describe the relevant flow processes. Initially, an Eulerian-Eulerian two-phase flow model was utilised to predict the internal nozzle flow under cavitating conditions. This model was weakly coupled with a Lagrangian spray model predicted the subsequent atomization and penetration of all individual spray plumes. The obtained results show that cavitation development within the upper layer holes is more intense than those formed within the lower layer nozzle holes; this is leading to higher injection rates from the lower layer nozzle holes that they also exhibit less cycle-to-cycle variations in the observed spray patterns.

Keywords

Diesel injector, coupled flow and spray, hole-to-hole variations, CFD, validation

1. Introduction

Despite efforts for electrification of the transport sector, the constantly increasing energy needs associated with the expansion of urbanization[1], population growth and the ever increasingly transportation needs in developing economies, are/will be met by medium/large diesel internal combustion engines (ICE), for which no foreseen electrification strategy is in place. As a result, liquid fossil fuels and in particular diesel, are expected to cover more than *2/3*^{rds} of the total energy

* Corresponding author: Fuqiang Luo, School of Automotive and Traffic Engineering, Jiangsu University, Zhenjiang 210213, China
Email: luofq@ujs.edu.cn

usage for transportation[2] in the next two decades. Currently, diesel engines are responsible for ~30wt% of soot and ~17% of man-made CO_2 emissions.[3] Despite the immense reduction achieved (>90% relative to 2000 levels), soot is one of the deadliest forms of air pollution: such particles inhaled at city centres, are linked to serious health effects, including premature death, heart attacks and strokes, as well as acute bronchitis and aggravated asthma among children.

Due to diesel fuel's strong impact on soot and NOx emissions, strict combustion emission regulations are imposed to diesel engines. One way of reducing emissions is to improve the injection and atomization characteristics of diesel fuel during engine operation. Fuel injectors are one of the major components of combustion engines as they control fuel delivery, atomisation, mixing and to a large extent the combustion process. Atomisation, in particular, is known to be influenced by the in-nozzle flow. Numerous studies have addressed experimentally and numerically the formation and development of turbulence and cavitation inside fuel injectors for various nozzle designs and their effect on atomization.[4–10] Despite considerable improvement in instrumentation technology, experimentation of the internal nozzle flow and spray breakup is challenging. Most of the relevant studies focus on scaled-up or simplified designs of real-size nozzles.[11] In order to control the duration of fuel injection in a reasonable range and obtain good spray atomization in heavy-duty high-pressure common rail diesel engines where large amounts of fuel per cycle are injected, the number of nozzle orifices are increased while they accommodate smaller hole diameters. However, as the number of orifices increase, the forming spray jets are easily interacting, and thus, limiting the fuel distribution. As a result, the space available for combustion in the engine are not fully utilized, thereby compromising the combustion quality. In addition, modern diesel engines are operated under high injection pressure ($> 2500 bar$) with injectors having small injection hole diameters of $90-120 \mu m$; these conditions pose significant difficulties in measuring and/or optically visualising the processes occurring in both the injector nozzle and within the high pressure/temperature combustion chamber. The majority of transparent real-size nozzle investigations have been performed in simplified single-hole geometries that generally confirm the presence of geometric-induced cavitation.[12–15] Still, quantification of the liquid volume fraction and differentiation between the vapour and gaseous cavitation is an open question. On the contrary, numerical simulations can provide insight regarding the flow dynamics at a resolution that cannot be obtained with today's experimental techniques. Some of the most recent work summarizing the relevant modelling approaches can be found in [16–18].

Using customized test rigs featuring transparent nozzles, injection rate measurements, cavitation and spray visualization techniques, researchers were able to investigate the internal flow and the subsequent spray development from various viewing angles. The Bosch measuring method[19] and the EFS mono-injection flow meter have been used to measure the injection rates regardless of the orifices numbers. This compromises the accuracy of the results since the influence of the individual nozzle holes on injection rate and spray formation are different (due to different hydraulic conditions). Although cavitation visualization provides detailed information regarding the cavitating flow within nozzles, it has only be used at injection pressures up to 1000bar with actual injector geometries, because the materials used to manufacture such nozzles cannot withstand higher pressures. However, both macroscopic and microscopic spray characteristics have been obtained using methods such as X-ray imaging techniques [10,20], Particle image velocimetry, Phase Doppler Anemometry and chemiluminescence apparatus.[21–23]

Given the limited quantitative information around the flow structure inside diesel injectors, fuel injection equipment manufacturers require robust predictive Computational Fluid Dynamics (CFD) tools, in order to understand the physical mechanisms taking place during injection. From a physical viewpoint, modelling of such flow conditions requires the fluid compressibility [24], mass transfer (cavitation, flash boiling, evaporation[25,26]) and heat transfer[27–29] to be taken into account, which increase the complexity as well as the computational cost of the simulations. Additionally, the fluid dynamics processes occur at high Reynolds number and therefore accounting for the effect of turbulent structures and vortex dynamics, is key in explaining how the injected fuel spray is formed[30–34]; this can only be resolved using very fine computational grids and scale resolving simulations, such as Large Eddy Simulation (LES), as initially presented in [35] for nozzle flows. Many different models have been developed for modelling cavitation; widely utilised approaches include the heterogeneous 'multi-fluid' model, the homogeneous 'mixture' model and the 'single-fluid' model. The multi-fluid approach can model non-equilibrium conditions between the phases i.e. each phase can have a different temperature, pressure and velocity.[36,37] The interaction between the phases is modelled using interphase exchange terms. In 'homogeneous' approaches, the slip velocity between the phases is neglected; this can be justified by the fact that even in the most extreme cases, the relative velocity between the two phases does not exceed 10% of the local velocity magnitude and only in very localised areas. The most widely utilised mixture approaches employ a transport equation for the mass/volume fraction of the secondary phase. In this type of models, the phase-change rate is controlled using a source term which is typically derived from the Rayleigh-Plesset (R-P) equation, as shown in [38–41]. A detailed review of such models can be found in [42] and [43]. The single-fluid approach for modelling cavitation uses an equation of state (EoS), which relates density and speed of sound with pressure and temperature.

Although the internal flow and spray characteristics of diesel injectors has been investigated to some extent (from literature), the complex relationship that governs the transition between the internal flow and spray development is yet to be fully understood. Furthermore, to the best of the author`s knowledge, computational analysis that studies the injection and spray characteristics from asymmetric nozzle holes (taking the effect of each nozzle hole concurrently) hasn't been researched extensively. Therefore, in this study, orifice-to-orifice variations in injection rate and spray development from a double-layer mini-SAC nozzle are investigated. A customized spray momentum flux experimental test rig was used to obtain the injection rates from each nozzle hole simultaneously, whereas for the spray, a customized test bench was used. For the simulations, independent computational analysis was conducted for the internal nozzle flow utilizing an homogenous mixture cavitation model while the spatial and temporal evolution of the flow from those simulations has been used an initial condition to an Eulerian-Lagrangian spray model resolving the subsequent spray development; the latter has been validated against the obtained experiments and has been further used to elucidate on the effect of nozzle flow on hole-to-hole spray variations.

2. Modelling

2.1 Geometry model

An eight-hole double layer Diesel injector used with heavy-duty vehicles has been utilised. Information for the actual nozzle geometry was obtained through X-ray Synchrotron radiation tomography technique. A sample of the obtained data for the geometry of the nozzle is shown in Fig. 1.

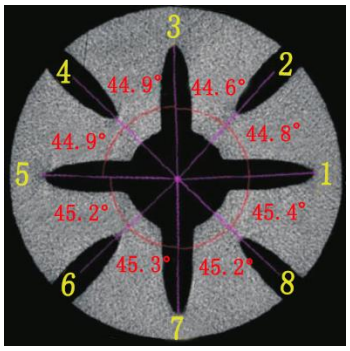

Fig.1 Cross-section image of the injection nozzle

The detailed geometric parameters of the nozzle including the hole lengths, inlet rounding corners, inlet and outlet diameters are shown in Table 1. All the nozzle holes are inclined with an angle of 75.5° as seen in Fig.2 (a) and (b); the inner shape of the needle tip is presented in Fig.2 (c). The lower layer holes are indicated as 1, 3, 5 and 7 and the upper layered hole as 2, 4, 6 and 8. The mean mass flow rates of the injector is 38.6 g/s at the working condition of 140MPa. The gap h between the upper layer and the lower layer nozzle holes is 0.12 mm. To ensure reliability of the results, the exact replica of the nozzle was numerically reconstructed from the X-ray images, taking into account all the disparities between holes.

Table 1 Geometric parameters

Nozzle holes	D_{in} /μm	D_{out} /μm	r /μm	L/mm
Lower 1,3,5,7	180.2	180.2	31	0.65
Upper 2,4,6,8	180.1	180.2	32	0.65

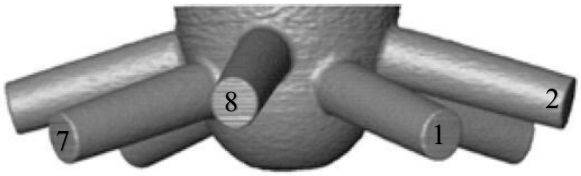

(a) schematic diagram obtained from X-ray technique

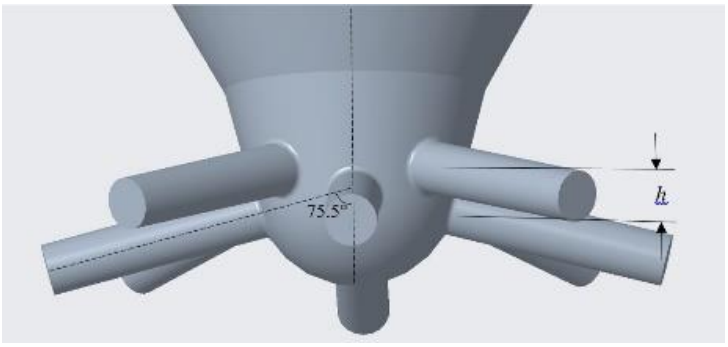

(b) the whole geometric model

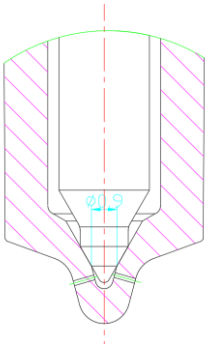

(c) 2D diagram showing the shape of the needle and the needle body

Fig.2 3D model of the injection nozzle

2.2 Coupled two-stage simulation approach

The coupled method is divided into two parts: the multiphase flow simulation within the injector and the spray jet simulation from the nozzle exit domain. Reynolds-Averaged Navier-Stokes (RANS) equations with the k-zeta-f turbulence model, where adopted in simulating spray development. The spray plume disintegration and development were computed using the models described recently by [44]. As an interface between the two simulations, the internal flow characteristics were used as the inlet boundary conditions for the subsequent spray simulation.

In order to achieve this, the calculated flow parameters representing the internal flow characteristics at the nozzle outlet (pressure, velocity field, vapour volume fraction and turbulent kinetic energy and its dissipation rate), were mapped on the grid cells and used as boundary conditions for the subsequent spray simulations.

2.3 Mathematical model

2.3.1 Nozzle modelling

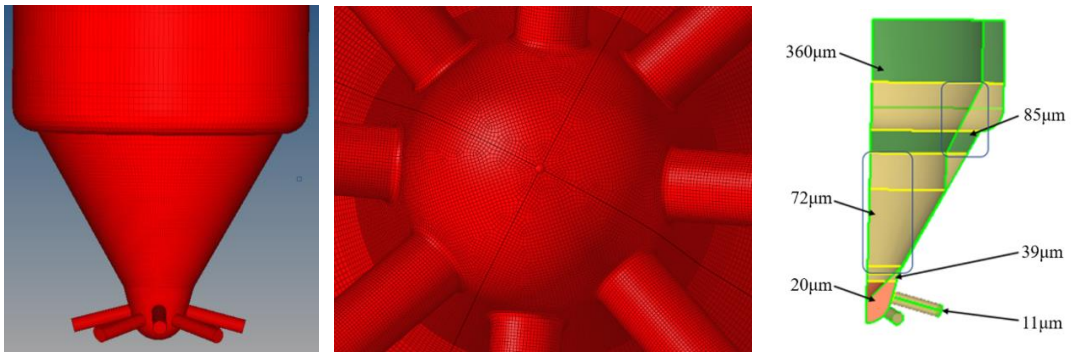

(a) front view (b) zoom view from the bottom (c) grid size

Fig.3 Diagram of computational grid

The whole nozzle model was discretized into ~400,000 hexahedral cells; numerical tests indicated that the mass flow rate was grid independent. In order to capture the transient cavitating flow within the nozzle, the mesh resolution was increased in critical areas, such as nozzle hole inlet and the needle seat, as it can be seen in Fig.3 (c). With the mean fuel flow velocity being around 550 m/s, an estimation of the Taylor length scale yielded around 2.1μm. In other words, the total mesh size that would be required for LES is ~10 million cells, while much smaller time steps will be needed; the difference in CPU time between LES and URANS adopted in this study is approximately 3 orders of magnitude, justifying the use of URANS. The inlet pressure, outlet pressure and temperature were set as 140 MPa, 2 MPa and 293.15 K respectively. The thermodynamic properties, of commercial B0 diesel fuel, assumed to be fixed, are listed in Table 2.

Table 2 Thermodynamic properties

Fuel Properties	Value
Density [kg/m^3]	830

Viscosity [mPa·s]	2.36
Saturation vapor pressure [Pa]	5540
Diesel vapor density [kg/m^3]	0.029
Diesel vapor viscosity [mPa·s]	1.8x10^{-3}

Fig.4 shows the assumed transient needle moving applied in the simulation. The needle movement was considered only in the vertical direction and it was represented by a cell-based mesh deformation method to ensure mass conservation; its possible eccentric movement was neglected as this is not known. The number of layer cells in the gap between the needle and the needle seat was 7, while the initial needle lift was set as 0.01 mm; the lift at full needle valve opening was 0.35 mm.

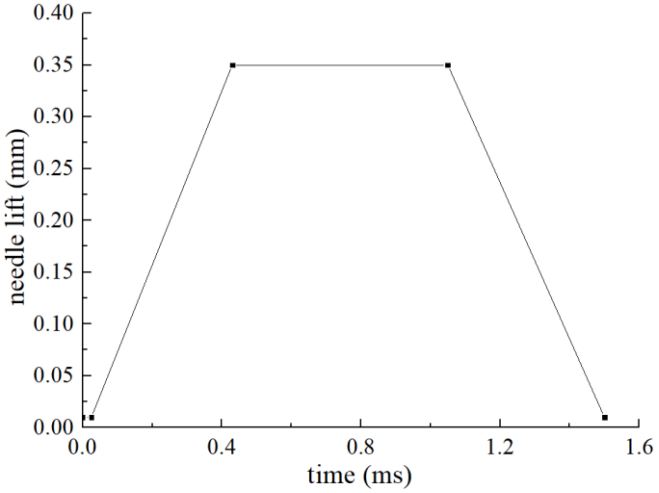

Fig.4 Needle lift curve

For the modelling of the internal fuel flow the Navier Stokes equations have been numerically solved, utilizing the commercial code AVL Fire. The pressure-based SIMPLE algorithm was used to couple the velocity and pressure fields. The in-nozzle flow simulation were governed by the mass (1), momentum (2) and energy conservation equations [45,46].

$$\frac{\partial \alpha_k \rho_k}{\partial t} + \nabla \cdot \alpha_k \rho_k v_k = \sum_{l=1, l \neq k}^{2} \Gamma_{kl} \tag{1}$$

$$\frac{\partial \alpha_k \rho_k v_k}{\partial t} + \nabla \cdot \alpha_k \rho_k v_k v_k = -\alpha_k \nabla p + \nabla \cdot \alpha_k (\tau_k + T_k^t) + \alpha_k \rho_k F + \sum_{l=1, l \neq k}^{2} M_{kl} + V_k \sum_{l=1, l \neq k}^{2} \Gamma_{kl} \tag{2}$$

$$\frac{\partial \alpha_k \rho_k v_k}{\partial t} + \nabla \cdot \alpha_k \rho_k v_k h_k = \nabla \cdot \alpha_k (q_k + q_k^t) + \alpha_k \rho_k q_k''' + \alpha_k \rho_k \cdot v_k + \nabla \cdot \alpha_k (\tau_k + \tau_k^t) \cdot v_k + \alpha_k \frac{\partial p}{\partial t} + \sum_{l=1, l \neq k}^{2} H_{kl} + h_k \sum_{l=1, l \neq k}^{2} \Gamma_{kl} \tag{3}$$

However, the volume fraction expression in Eq. 4 has to be satisfied

$$\sum_{k=1}^{2} \boldsymbol{\alpha_k} = \mathbf{1} \tag{4}$$

k represents the phase k, i.e. 1 for gas phase while 2 for liquid phase. α_k is the volume fraction of phase k, ρ_k is phase k density, v_k is phase k velocity, Γ_{kl} is the interfacial mass exchange between phases k and l, T_k^t is phase k Reynolds stress, and M_{kl} is the momentum interfacial interaction between phases k and l.[47]

The boundary conditions of the nozzle inlet and all orifices outlets were set as pressure boundary conditions, in order to capture the dynamic effects of cavitation phenomenon within nozzles. The interfacial exchanges in terms of momentum and mass within the fluids were computed with a drag model[44] and a linear mass exchange model considering cavitation[47] respectively. More specifically, the mass interfacial exchange was achieved through the linearized Rayleigh's cavitation model, derived from linearizing Equation 5 and 6 below:

$$\Gamma_{21} = \rho_2 N''' 4\pi R^2 \dot{R} = -\Gamma_{12} \tag{5}$$

$$\Gamma_{21} = \frac{1}{C_{CR}} sign(\Delta p) 3.95 \frac{\rho_1}{\sqrt{\rho_2}} N'''^{\frac{1}{3}} \alpha_1^{\frac{2}{3}} |\Delta p|^{\frac{1}{2}} = -\Gamma_{12} \tag{6}$$

where Δp, R and N''' and are the effective pressure differences, bubble radius and the bubble number density. The bubble radius time derivative from the Rayleigh's equation was performed with the expression

$$R\ddot{R} + \frac{3}{2}\dot{R}^2 = \frac{\Delta p}{\rho_2} \tag{7}$$

The momentum interfacial exchange (M_{kl}) was modeled with the equation

$$M_{kl} = C_D \frac{1}{8} \rho_k A_i''' |v_r| v_r + C_{TD} \rho_k k_k \nabla \alpha_l = -M_{lk} \tag{8}$$

Where C_D is the drag coefficient of the liquid droplets, A_i''' is the interfacial area density, v_r is the relative velocity and C_{TD} is the turbulence dispersion coefficient.[48]

The 4-equations k-zeta-f turbulent model, developed from the k-ε two-equation model, was adopted for capturing the turbulence phenomenon within the two-phase flow. The k-zeta-f model replicates turbulence and its interactions more accurately and with much more stability than the popular k-ε model [49]; however, it requires longer computation time. The basic expressions of the model are the turbulent kinetic energy (Eq. 9), its dissipation rate (Eq.10), the velocity scale (Eq. 11) and the elliptical function (Eq. 12).

$$\frac{\partial \alpha_k \rho_k k_k}{\partial t} + \nabla \cdot \alpha_k \rho_k v_k k_k = \nabla \cdot \alpha_k \left(\mu_k + \frac{\mu_k^t}{\sigma_k}\right) \nabla k_k + \alpha_k \mathrm{P}_k - \alpha_k \rho_k \varepsilon_k + \sum_{l=1, l \neq k}^{2} K_{kl} + k_k \sum_{l=1, l \neq k}^{2} \Gamma_{kl} \tag{9}$$

$$\frac{\partial \alpha_k \rho_k \varepsilon_k}{\partial t} + \nabla \cdot \alpha_k \rho_k v_k \varepsilon_k = \nabla \cdot \alpha_k \left(\mu_k + \frac{\mu_k^t}{\sigma_k}\right) \nabla \varepsilon_k + \sum_{l=1, l \neq k}^{2} D_{kl} + \varepsilon_k \sum_{l=1, l \neq k}^{2} \Gamma_{kl} + \alpha_k C_1 \mathrm{P}_k \frac{\varepsilon_k}{k_k} - \alpha_k C_2 \rho_k \frac{\varepsilon_k^2}{k_k} + \alpha_k C_4 \, \rho_{\,k} \varepsilon_k \nabla \cdot v_k \tag{10}$$

$$\frac{\partial \alpha_k \rho_k \zeta_k}{\partial t} + \nabla \cdot \alpha_k \rho_k v_k \zeta_k = \nabla \cdot \alpha_k \left(\mu_k + \frac{\mu_k^t}{\sigma_k}\right) \nabla \zeta_k + \zeta_k \sum_{l=1, l \neq k}^{2} \Gamma_{kl} - \alpha_k \mathrm{P}_k \frac{\zeta_k}{k_k} + \alpha_k f_k \tag{11}$$

$$f_k = L_k^2 \nabla^2 f_k - \frac{1}{T_k}\left(C_1 - 1 + C_2 \frac{P_k}{\varepsilon_k}\right)\left(\zeta_k - \frac{2}{3}\right) \tag{12}$$

where, k_k is the turbulence kinetic energy at phase k, ε_k is the diffusivity of the turbulence kinetic energy at phase k, ζ_k is the velocity scales ratio at phase k, f_k is the elliptic function at phase k, P_k is the production term of the turbulence kinetic energy due to shear and $P_{B,k}$ is the generation component of the turbulence kinetic energy caused by buoyancy. The Prandtl number for the turbulence kinetic energy is σ_k, K_{k1} is the component of transmission between phases k and l, σ_ε is the Prandtl number for the ε equation and C_1, C_2, C_3, C_4 are constants. D_{k1} is the interfacial e deled with hybrid wall equations. The turbulence for the near-wall regions were modeled notwithstanding wall equations. Further analyzing of the equations are presented in [47].

The spatial discretization of the momentum equation was performed by a bounded central differential second–order scheme, while the discretization of the continuity equation was achieved with the MINMOD scheme. The blending factor was set as 0.5 for momentum discretization in order to achieve a compromise between computational accuracy and convergence. Time advancement was performed with a second-order backward differencing scheme, in order to capture the complex turbulence structures within the nozzle.[44,50,51] Because of the different resolution in time and space, the time step interval was set as 1×10^{-6}s, which took the whole simulation 360 CPU·h using 24 processors.

2.3.2 Spray modelling

For the spray simulation, the injector was located in the top middle of the spray chamber model, which was built as a cylinder with a length of 0.04 m and a diameter of 0.08 m. The chamber was discretized into ~2million cells. The simulation was implemented in a non-evaporating condition at the same temperature and pressure settings as those from experiment.

At the exit of orifices the local distribution parameters of the flow field variables, such as the

turbulent kinetic energy and the vapor distribution, were captured and used as the inlet boundary conditions for the subsequent spray simulation. The 3D results of the flow field variables at the time step of 1.25ms are as shown in Fig. 5. In figure, distinct differences can be observed across the interface. These differences keep changing and therefore influence the breakup behavior and penetration of the spray jets from the various orifices.

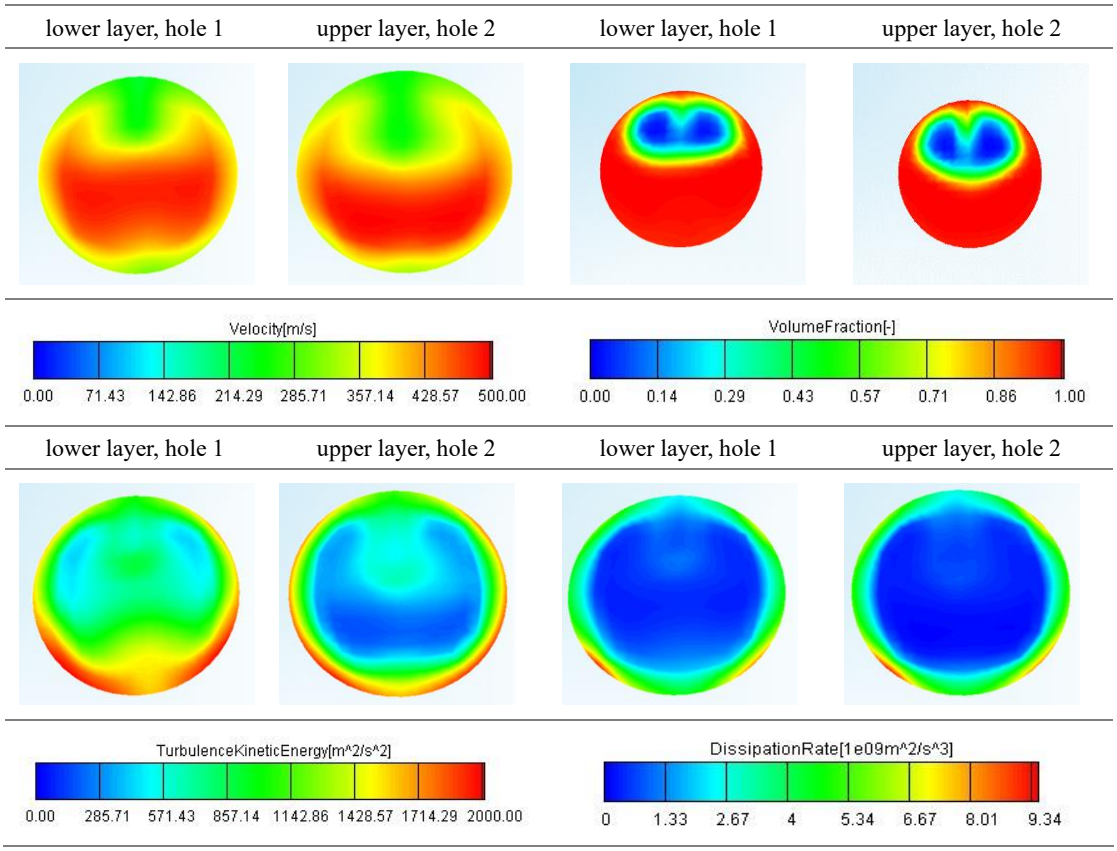

Fig.5 Flow characteristics at the exit of orifices at 1.25ms

Primary breakup

The blob injection model was selected for the primary breakup model in this study because it could couple the upstream internal flow characteristics to the downstream spray simulation [52]. The model considers that the fragment of droplets is dominated by the competitive process between the turbulence caused by cavitation and the aerodynamic-induced breakup.

Under the aerodynamic breakup mechanism, the breakup of the liquid core was modeled with:

$$\left(\frac{dr}{dt}\right)_a = R_a = -\frac{(r - r_a)}{C_2 \cdot \tau_a} \tag{13}$$

where r is the actual droplet radius, C_1 and C_2 are constants used for adjusting breakup time and the characteristic droplet radius, r_a is the characteristic droplet radius, τ_a is the breakup time and Λ is the dominant aerodynamic wavelength. The subsequent breakup rate of droplets with regards to turbulent length scale (r_T) was modeled with:

$$\frac{dR}{dt} = -\frac{r - C_3 r_T}{C_4 \tilde{\tau}_T} \quad (14)$$

where

$$r_T = C_\mu^{0.75} \frac{k^{1.5}}{\varepsilon} \quad (15)$$

$$\tau_T = C_\mu \frac{k}{\varepsilon} \quad (16)$$

C_μ and C_4 are model constants and $\tilde{\tau}_T = k/\varepsilon$.

Under the turbulence and cavitation breakup mechanism, the geometric and flow dynamic properties of the orifices provides the relevant local parameters. This ensures that the transient conditions of the cavitating flow were captured together with their influence on droplet breakup. By negligible diffusion effects, the expressions for the induced turbulence in the liquid fuel core are:

$$\frac{dk}{dt} = -\varepsilon + S_k \quad (17)$$

$$\frac{d\varepsilon}{dt} = -C \cdot \frac{\varepsilon}{k} \cdot (\varepsilon - S_k) \quad (18)$$

where S_k is the cavitation source term and C is a constant.

Secondary Break up

Secondary breakup of droplets occurs when the aerodynamic breakup mechanism dominates the turbulent-induced and cavitation breakup mechanism.[48] For a high pressure diesel engine, the KH-RT model has been shown to give more accurate results than WAVE and TAB models, hence it was adopted during this study. The values of the constant for this study has been listed in the Table 3.[53]

Table 3 Constant settings of KH-RT model

Model constants	Value
C1	0.61
C2	18
C3	30
C4	2.5
C5	1
C6	0.3
C7	0.03
C8	0.188

2.3.3 Mesh sensitive analysis

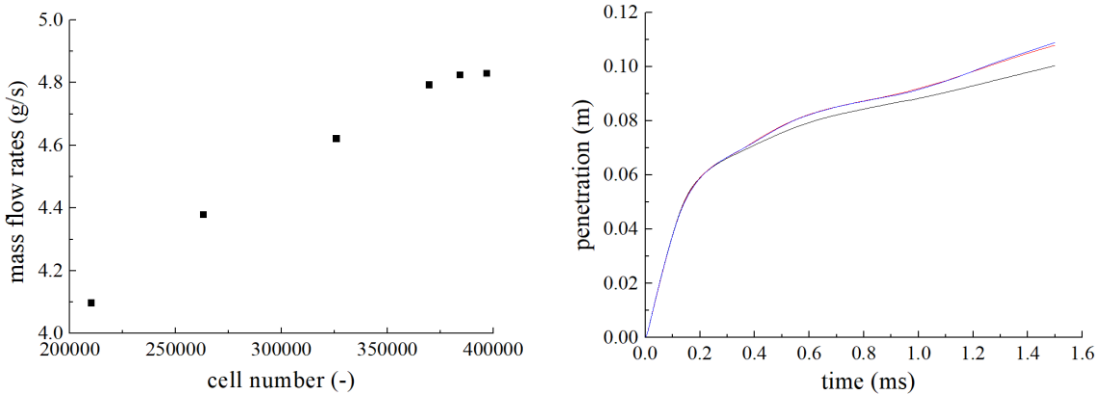

(a) internal-flow (b) spray pattern

Fig.6 Mesh sensitive analysis for flow and spray domains

To ensure the simulation results of flow and spray domain are independence of the mesh size, various tests have been performed as shown in Fig. 6 (a) and (b). It can be seen from these figures that grid convergence was attained for the internal flow at around 400,000 cells, while for the spray domain, convergence was attained with about 2 million cells.

3. Experiment Establishment and validation

3.1 Internal flow characteristics

The measurement of injection rates among each nozzle holes were conducted on a customized test rig based on the spray momentum flux. Detailed information about the test method and the test bench are presented in the [54–56]. The experiment was conducted with the injection pressure of 140MPa and back pressure of 2MPa. Validation was carried out by comparing experimental and simulation injection rates at the exit of each orifice; the comparisons are presented in Fig. 7.

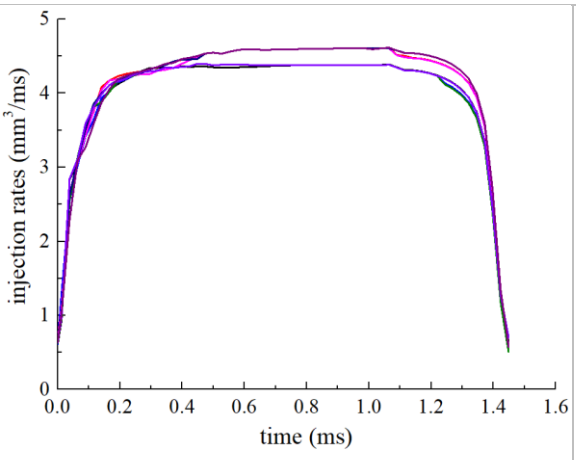

(a) simulation results

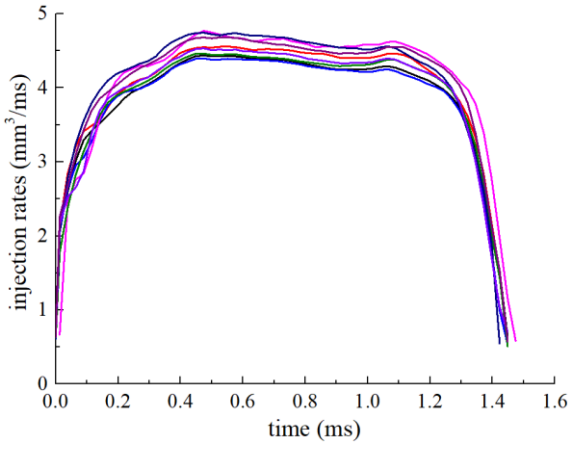

(b) experimental results

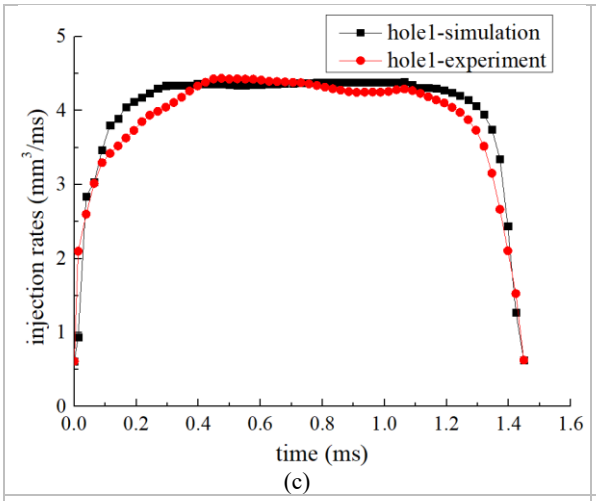
hole1-simulation
hole1-experiment
injection rates (mm3/ms)
time (ms)
(c)

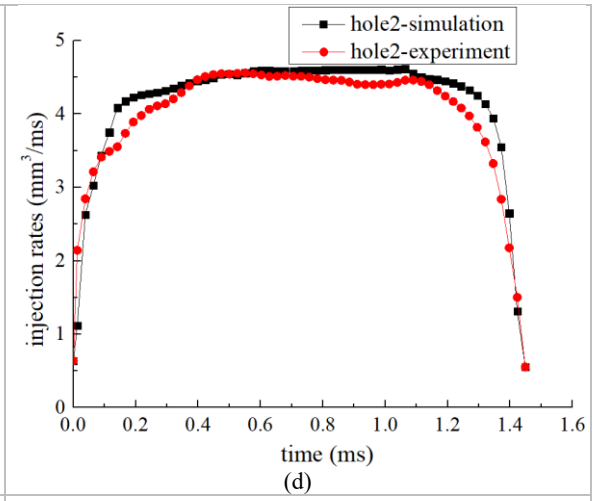
hole2-simulation
hole2-experiment
injection rates (mm3/ms)
time (ms)
(d)

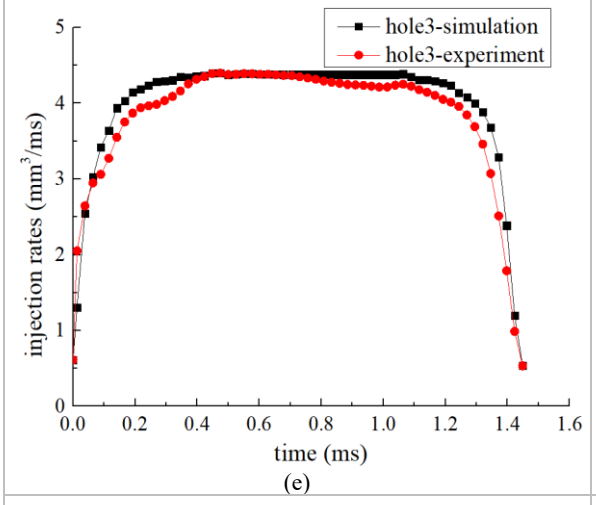
hole3-simulation
hole3-experiment
injection rates (mm3/ms)
time (ms)
(e)

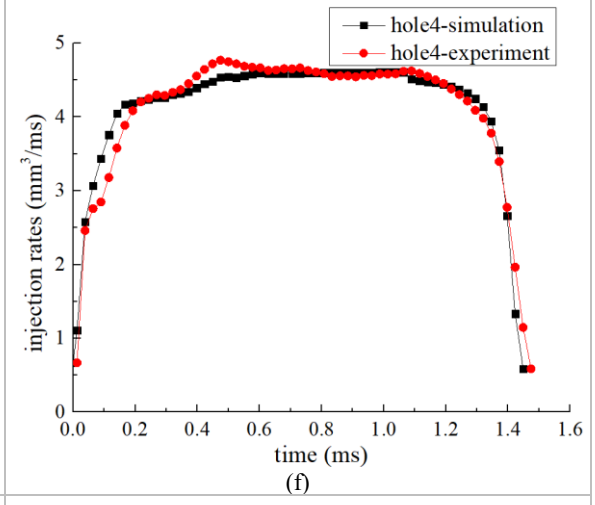
hole4-simulation
hole4-experiment
injection rates (mm3/ms)
time (ms)
(f)

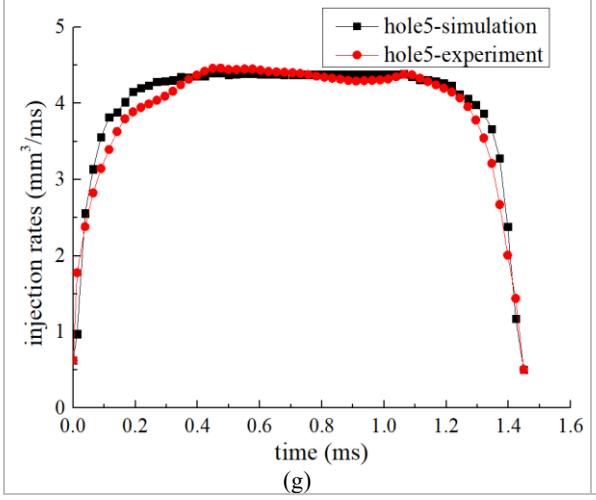
hole5-simulation
hole5-experiment
injection rates (mm3/ms)
time (ms)
(g)

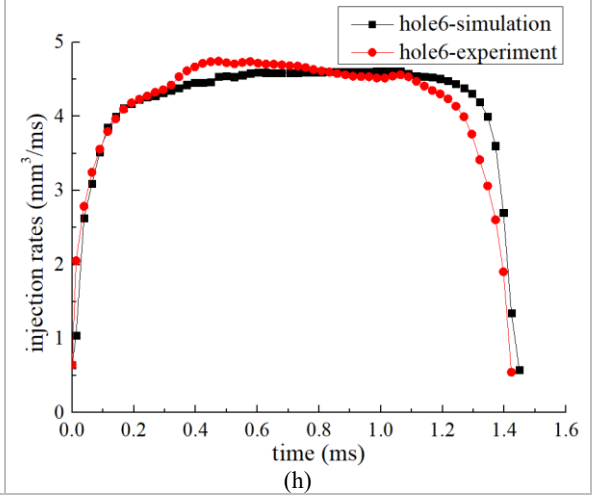
hole6-simulation
hole6-experiment
injection rates (mm3/ms)
time (ms)
(h)

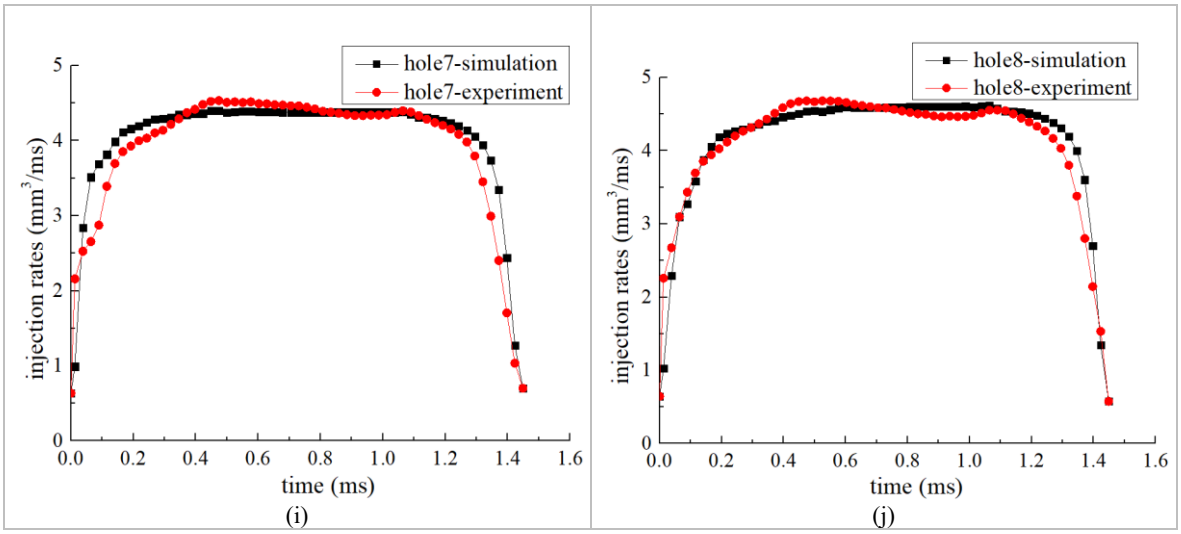

Fig.7 Comparison between simulation and experimental results for the injection rate from individual injection holes

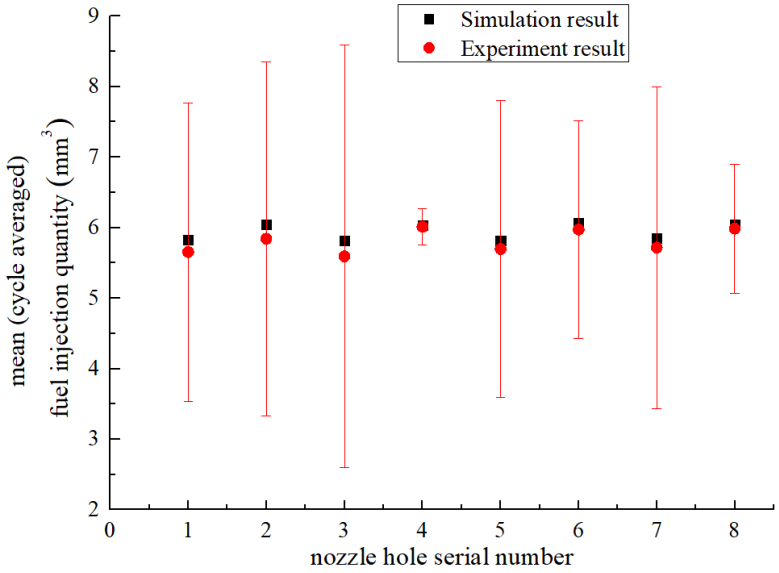

Fig.8 Comparison of hole-to-hole injection quantities and their standard deviation over injection cycles

Fig.7 and Fig.8 show the comparison between the simulation and experiment results at the injection pressure of 140MPa with 2MPa back pressure. From Fig.7, similar trends were present in both measured and simulated hole-to-hole injection rates. To compute the deviation (error) between the computational and experimental results, an expression in equation (17) was used:

$$\Delta_{hole} = \frac{q_{simulation} - q_{measure}}{q_{measure}} \times 100\% \quad (17)$$

Fig.8 shows that, the largest relative error of cycle fuel injection quantities between the simulation and experiment is less than 3% (at orifice 3). This means that the computational model's accuracy is within acceptable limits.

In addition, to quantify the relative discrepancy in cycle fuel injection quantity between the upper and the lower layer nozzle holes, equation (18) was introduced:

$$\Delta = \frac{Q_{lower} - Q_{upper}}{Q_{lower}} \times 100\% \quad (18)$$

where Q_{lower} is the total injection quantity of the lower layered holes，Q_{upper} is the total injection quantity of the upper layer holes. The result show that the fuel injection quantities of the lower layer orifices are 6-13% higher than the upper layer orifices. This can be attributed to the smaller flow resistance the fuel experiences as a result of the fuel's gentle entrance into the lower layer orifices.

3.2 Spray patterns

EFS8400 spray test bench, a constant volume chamber, high speed CCD camera system and the common-rail fuel injection system-BOSCH MOEHWALD-CA4000, were used to acquire spray images and spray jet characteristics through Schlieren method at different injection pressures.[57] Synchronization trigger was adopted to synchronize the working process of the CCD cameras and the fuel injection system. Ambient pressure in the constant volume chamber was provided by stable nitrogen. The maximum pressure of the chamber is 5.2 MPa with a temperature of 293.15±2K. Two high speed CCD cameras were installed at the side and the bottom of the constant volume chamber respectively, to photograph the spray shadow through the quartz window. Details on the spray test experimental platform could be found in [57], the injection duration was set at 1.5ms.

Fig.9 shows the simulation results of individual jet penetration for the 8-hole injector at 140 MPa injection pressure and a back pressure of 2MPa (same with internal flow simulation). It is obvious from the figure that, the penetration of the spray jets from the lower layer orifices (1,3,5,7) is much faster than those from the upper layer orifices (2,4,6,8). The difference in spray penetration between the two layers could reach 30% or more. However, the differences in their respective injection rates is between 4% to 8%, as shown in Fig.7.

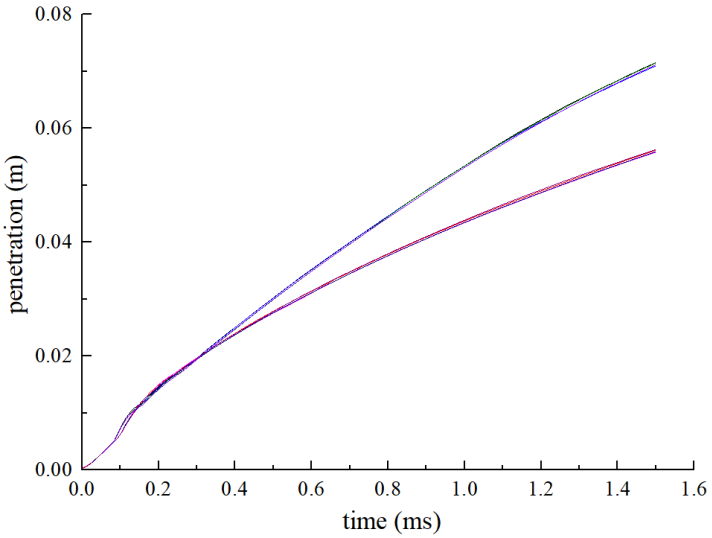

Fig.9 Simulated penetration results of individual spray plumes

Although there are some discrepancies in injection rates among the eight nozzle offices, the jet penetration results of the two layered holes (i.e. penetrations of hole 1,3,5,7 and hole 2,4,6,8 respectively, as shown in Fig.9) showed acceptable levels of consistency with marginal differences. Therefore, hole 1 from the lower layer and hole 2 from the upper layer were compared with experimental data for validation.

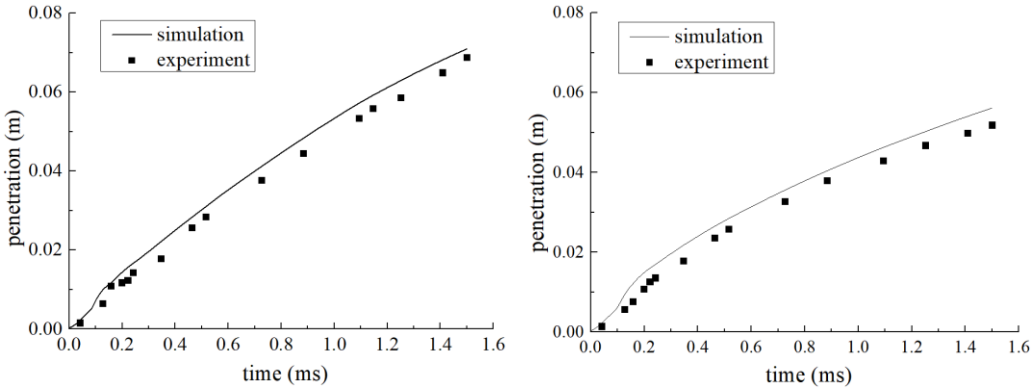

(a) hole 1 (b) hole 2

Fig.10 Comparison of hole-to-hole spray penetration

Fig. 10 presents the divergence between the experiment and simulated spray jet penetration results. The numerical results showed good consistency against the experimental results, even though they are slightly higher in magnitude. Also, the deviation between the two is larger during the initial stages of injection, and then gradually reduces at longer penetration distances; the deviations are all within acceptable limits (10 %). It should be mentioned that constant inlet boundary condition was set for the internal flow simulation instead of the varying conditions that pertains in reality.

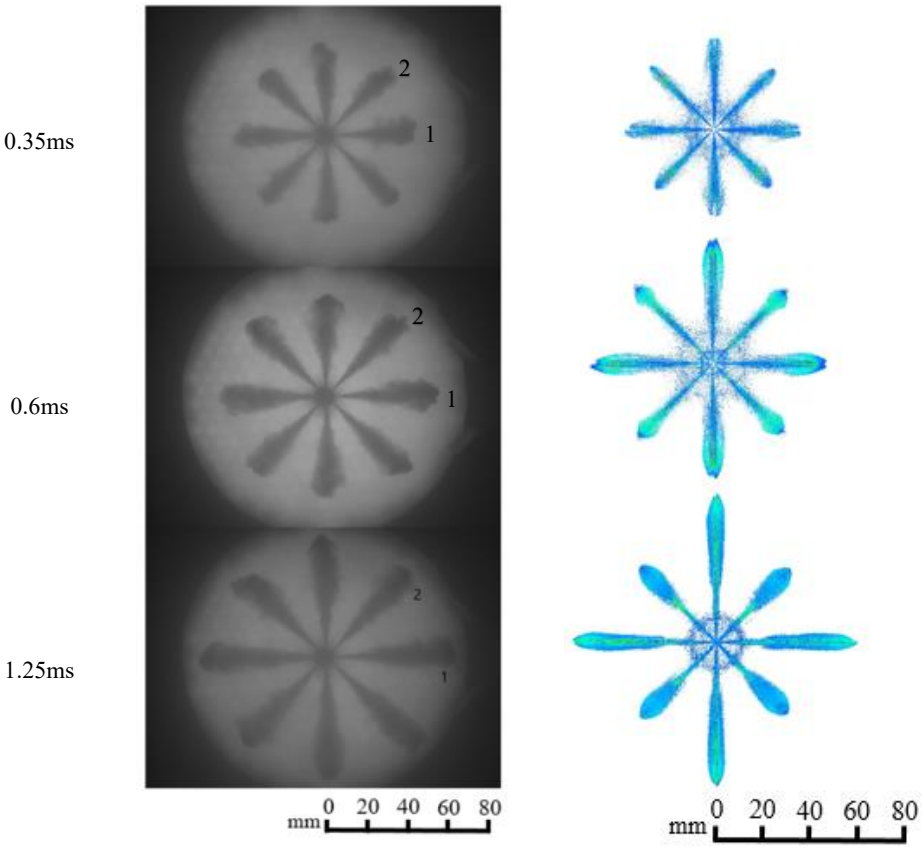

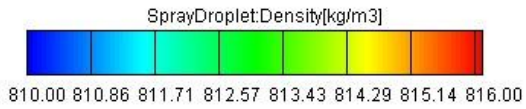

Fig.11 Contrast image of experiment and simulation

The experimental and numerical 3D spray images (at the inlet pressure of 140 MPa with a back pressure of 2 MPa) are shown in Fig. 11. Hole 1 and hole 2 are marked in the experimental images. The others follow the same numbering pattern in the counterclockwise direction. From the images, it is clear that the spray development from simulation and experiment followed similar patterns. Furthermore, the spray penetrations of hole 1,3,5,7 are larger than those of hole 2,4,6,8, while the spray cone angles of hole 1,3,5,7 are also slightly bigger. Fig.9 to Fig.11 show good consistency between computational and experimental results, implying that the coupled model could be used for further analysis in both cavitation flow within the injector and spray jet development.

4. Results and discussion

4.1 in-nozzle flow characteristics

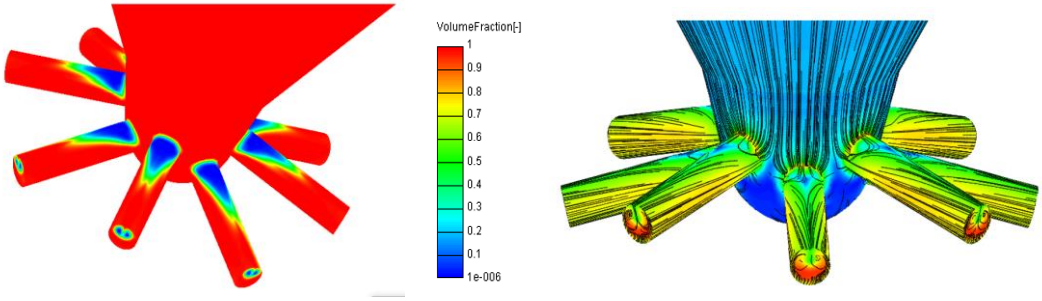

(a) (b)

Fig.12 (a) Cavitation distribution; (b) fuel velocity streamline at full needle lift

Cavitation distribution and fuel velocity streamlines in the double-layer nozzle at maximum needle lift are shown in Fig. 12. The cavitation distributions and flow streamlines are both highly symmetric with negligible differences. When the needle valve is fully opened, the cavitation in both the upper and the lower layered holes occurs in the upper part of the orifices. In addition, cavitation occupies a relative larger area in the upper layer nozzle holes than the lower layer ones.

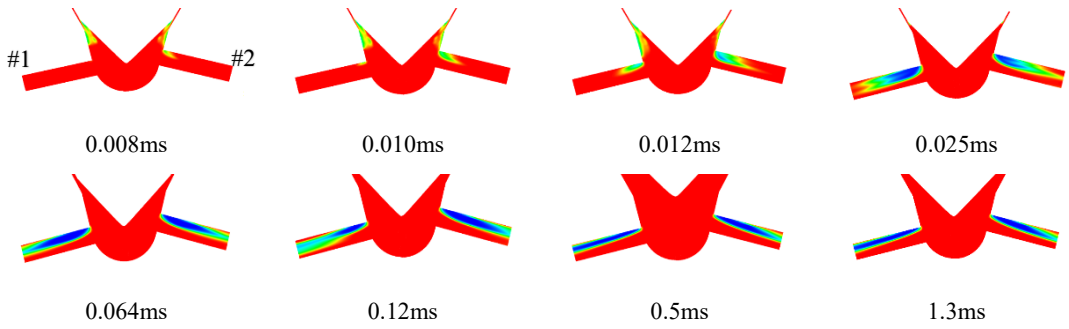

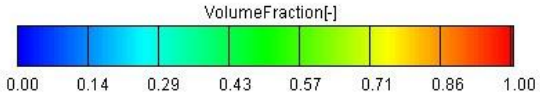

Fig.13 Variation of cavitation development with the time

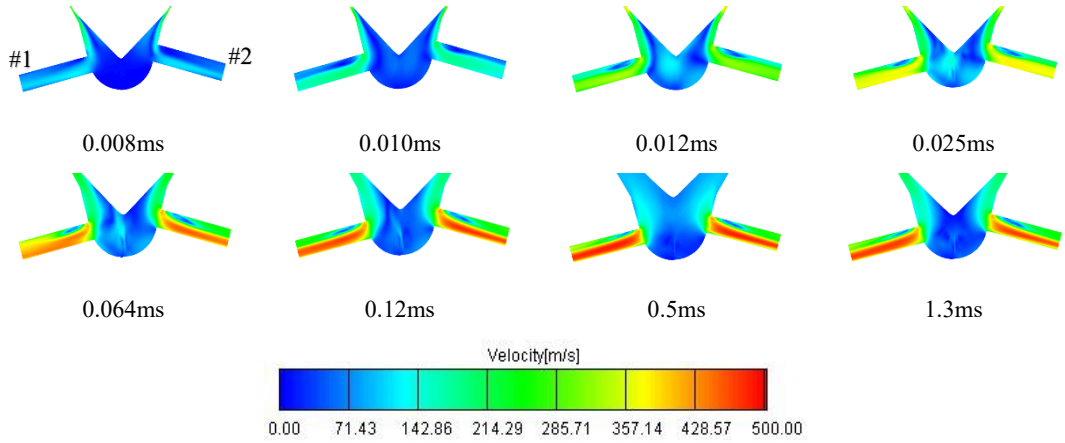

Fig.14 Variation of velocity magnitude with the time

Fig.13 and Fig.14 shows the variation of cavitation and velocity flow field distribution between the upper and lower layer nozzle holes. To better visualize the flow characteristics within the injector, hole 2 is rotated to make the same plane as hole 1. As shown in these figures, cavitation occurs earlier in the upper layered nozzle holes and develops faster as compared to cavitation development in the lower layered nozzle holes. In addition, the fuel velocity in the upper layered nozzle holes is slightly faster. At full needle lift, the fuel flow velocity distributions of the upper layered nozzle holes is also less uniform. The cumulative effect of these discrepancies results in the manifestation of higher degree of cavitation developments in the upper layered nozzle holes than the cavitation developments in the lower layered nozzle holes. Furthermore, the acuteness of the upper layer hole means that cavitation development at their entry sections will be more developed than those at the less acute lower layered holes.

4.2 Spray development

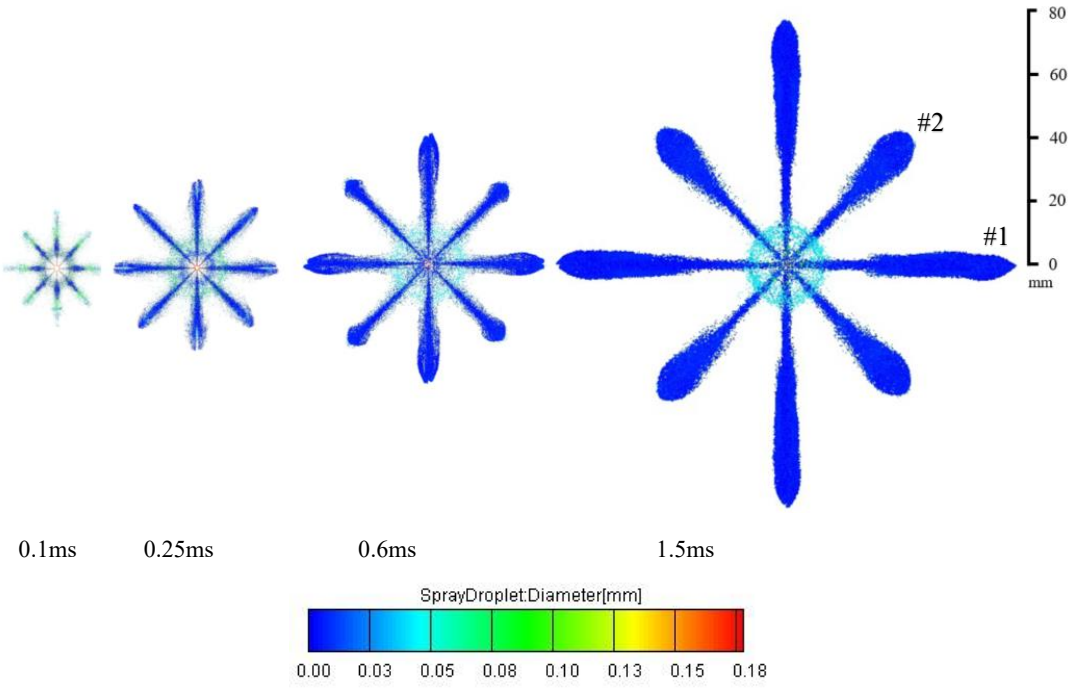

Fig.15 Spray droplet diameter with the time

Fig. 15 and 16 represent the spray jet development at different times. In Fig.15, the spray droplet diameter is large at the initial stages of the injection. The spray jet penetration was changed gradually with the evolution of the injection progress. Furthermore, the droplet size continues to decrease due to subsequent droplet breakups. After 0.25ms from the start of injection, the number of the spray droplets increases significantly.

The shape of individual spray jets starts to differentiate after 0.1ms, while the difference become more apparent after 0.25ms. The spray jet penetration from the upper and lower layer holes remain almost the same before 0.25ms. At the end of injection, the droplet distribution from the lower layer holes are more uniform than the distribution from the upper layer nozzle holes.

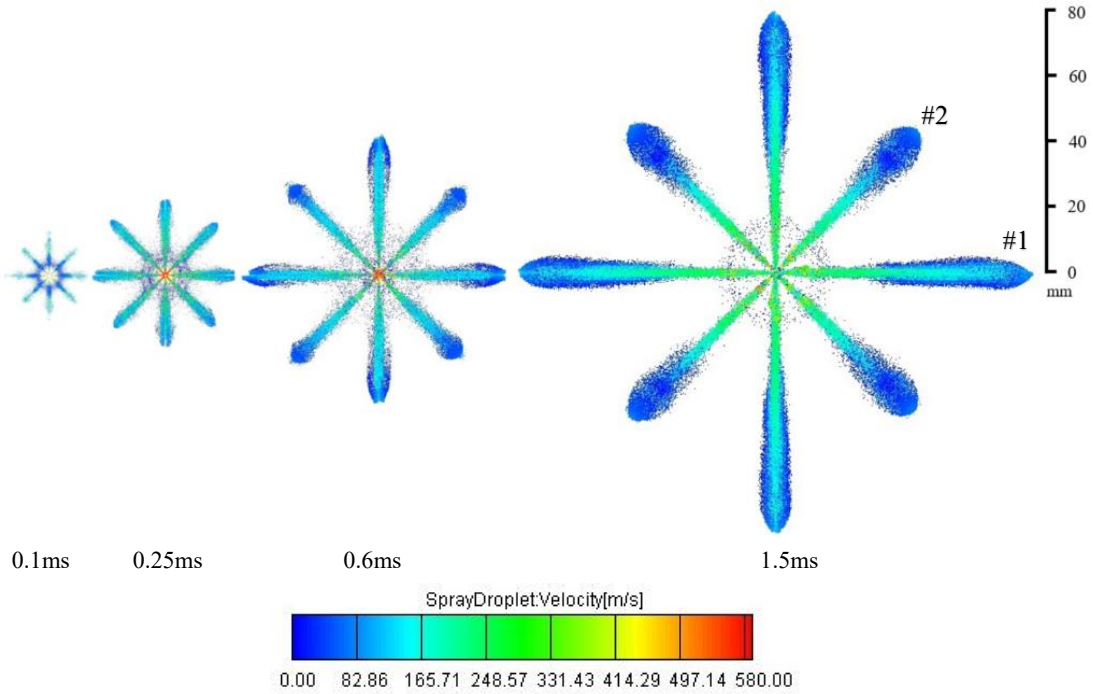

Fig.16 Spray velocity field with the time

The spray velocity field is represented in Fig.16; discrepancies can be seen. In the direction of the spray jet axis, the droplet velocity decreases outwards along the central axis, because of the larger aerodynamic influence on the droplets in the far-field of the spray domain. The jet velocity in the near nozzle domain, increases as the spray progresses, reaching around a maximum speed of 580 m/s at 0.6 m/s after start of injection, and ends at 283.7 m/s. While in the far field of the spray domain, the velocities of the droplets are much smaller than those around the near nozzle domain (less than 100 m/s).

5. Conclusions

A double-layer 8-hole heavy-duty diesel engine nozzle geometry derived from X-ray scans and featuring all geometrical differences between the individual injection holes was used for the characterization of hole-to-hole variation on spray formation. This was achieved through numerical simulations. Internal nozzle flow was simulated (using RANS two-phase flow model) and the results, interfaced as inlet boundary conditions during spray simulation, using the Euler-Lagrangian approach. The technique was then used to predict spray development after validation. Model validation was obtained against momentum fluxes from all eight individual holes as well as the corresponding spray tip penetration rates. The following conclusion were arrived at from further analysis:

1) Injection rate as well as spray penetration time histories from both simulation and experiment follows almost the same trend overall. The accuracy of the established model in predicting flow characteristics and spray patterns are high and within acceptable limits (less than 5% in flow and within 10% in spray).

2) From both experiments and simulations, the injection rate and the cycle fuel injection quantities

of the lower layer nozzle holes were between 4 – 8 % higher than the cycle fuel injection quantities of the upper layer nozzle holes. The differences in spray penetration from the lower layer holes and the upper layer ones reached more than 30%.

3) The acuteness of the upper layer nozzle holes contributed to the formation of a higher degree of cavitation development in them and also high spray droplet velocities as compared to the less acute lower layer nozzle holes.

Acknowledgement

This work was supported by the National Natural Science Foundation of China (No. 51476072), and the Chinese Scholarship Council (CSC No. 201808320261).

Reference

1. Deb M, Sastry GRK, Bose PK, Banerjee R. An experimental study on combustion, performance and emission analysis of a single cylinder, 4-stroke DI-diesel engine using hydrogen in dual fuel mode of operation. *Int J Hydrogen Energy*. 2015;40(27):8586-8598.
2. Reitz RD, Ogawa H, Payri R, et al. IJER editorial: The future of the internal combustion engine. *Int J Engine Res*. 2020;21(1):3-10.
3. Karathanassis IK, Koukouvinis P, Gavaises M. Comparative evaluation of phase-change mechanisms for the prediction of flashing flows. *Int J Multiph Flow*. 2017;95:257-270.
4. Gavaises M, Papoulias D, Andriotis A, Giannadakis E, Theodorakakos A. Link Between Cavitation Development and Erosion Damage in Diesel Injector Nozzles. *SAE Tech Pap 2007-01-0246*. Vol 2007. ; 2007:776-790.
5. Payri F, Bermúdez V, Payri R, Salvador FJ. The influence of cavitation on the internal flow and the spray characteristics in diesel injection nozzles. *Fuel*. 2004;83(4-5):419-431.
6. He Z, Zhou H, Duan L, Xu M, Chen Z, Cao T. Effects of nozzle geometries and needle lift on steadier string cavitation and larger spray angle in common rail diesel injector. *Int J Engine Res*. July 2020;1-16.
7. Prasetya R, Sou A, Oki J, Nakashima A. Three-dimensional flow structure and string cavitation in a fuel injector and their effects on discharged liquid jet. *Int J Engine Res*. Mar. 2019;1-14.
8. Arcoumanis C, Gavaises M, Argueyrolles B, Galzin F. Modeling of Pressure-Swirl Atomizers for GDI Engines. *SAE Trans*. 1999;108:516-532.
9. Giannadakis E, Papoulias D, Theodorakakos A, Gavaises M. Simulation of cavitation in outward-opening piezo-type pintle injector nozzles. *Proc Inst Mech Eng Part D J Automob Eng*. 2008;222(10):1895-1910.
10. Naseri H, Trickett K, Mitroglou N, et al. Turbulence and Cavitation Suppression by Quaternary Ammonium Salt Additives. *Sci Rep*. 2018;8(1):1-15.
11. Hayashi T, Suzuki M, Ikemoto M. Visualization of Internal Flow and Spray Formation with Real Size Diesel Nozzle. *12th Triennial International Conference on Liquid Atomization and Spray Systems (ICLASS)*, Heidelberg,

Germany, 2012.
12. Reid BA, Gavaises M, Mitroglou N, et al. On the formation of string cavitation inside fuel injectors. *Exp Fluids*. 2014;55(1):1-8.
13. Lockett RD, Bonifacio A. Hydrodynamic luminescence in a model diesel injector return valve. *Int J Engine Res*. Aug. 2019;1-12.
14. Mitroglou N, McLorn M, Gavaises M, Soteriou C, Winterbourne M. Instantaneous and ensemble average cavitation structures in Diesel micro-channel flow orifices. *Fuel*. 2014;116:736-742.
15. Fitzgerald RP, Vecchia G Della, Peraza JE, Martin GC, Térmicos M, Politècnica U. Features of Internal Flow and Spray for a Multi-Hole Transparent Diesel Fuel Injector Tip. *ILASS–Europe 2019, 29th Conf Liq At Spray Syst 2-4 Sept 2019, Paris, Fr*. 2019;(September):2-4.
16. Gomez Santos E, Shi J, Gavaises M, Soteriou C, Winterbourn M, Bauer W. Investigation of cavitation and air entrainment during pilot injection in real-size multi-hole diesel nozzles. *Fuel*. 2020;263:116746.
17. Martin Gold, Richard Pearson, Jack Turner, Dan Sykes, Viacheslav Stetsyuk, Guillaume de Sercey, Cyril Crua, Mithun Girija Murali, Foivos Koukouvinis, Manolis Gavaises. Simulation and Measurement of Transient Fluid Phenomena within Diesel Injection. *SAE Tech Pap 2019-01-0066,* 2019.
18. Mithun MG, Koukouvinis P, Gavaises M. Numerical simulation of cavitation and atomization using a fully compressible three-phase model. *Phys Rev Fluids*. 2018;3(6):0-3.
19. Ferrari A, Zhang T. Benchmark between Bosch and Zeuch method–based flowmeters for the measurement of the fuel injection rate. *Int J Engine Res*. Mar. 2019;1-12.
20. Karathanassis IK, Trickett K, Koukouvinis P, Wang J, Barbour R, Gavaises M. Illustrating the effect of viscoelastic additives on cavitation and turbulence with X-ray imaging. *Sci Rep*. 2018;8(1):1-15.
21. Pastor J, Garcia-Oliver JM, Garcia A, Zhong W, Micó C, Xuan T. An Experimental Study on Diesel Spray Injection into a Non-Quiescent Chamber. *SAE Int J Fuels Lubr*. 2017;10(2):394-406.
22. Matusik KE, Sforzo BA, Seong HJ, Duke D, Kastengren AL, Ilavsky J, Powell CF. X-ray measurements of fuel spray specific surface area and sauter mean diameter for cavitating and non-cavitating diesel sprays. *At Sprays*. 2019;29(3):199-216.
23. Ajrouche H, Nilaphai O, Moreau B, Hespel C, Foucher F, Mounaïm-rousselle C. Engine Combustion Network (ECN): Characterization and comparison of Diesel spray combustion in new high-pressure and high-temperature chamber. *19th Annu Conf Liq At Spray Syst ILASS-Asia*. 2017;(October):1-4.
24. Koukouvinis P, Gavaises M, Li J, Wang L. Large Eddy Simulation of Diesel injector including cavitation effects and correlation to erosion damage. *Fuel*. 2016;175:26-39.
25. Zhou X, Li T, Wei Y, Wang N. Scaling liquid penetration in evaporating sprays for different size diesel engines. *Int J Engine Res*. Dec. 2019;1-16.

26. Nsikane DM, Vogiatzaki K, Morgan RE, et al. Novel approach for adaptive coefficient tuning for the simulation of evaporating high-speed sprays injected into a high-temperature and high-pressure environment. *Int J Engine Res*. 2020;21(7):1162-1179.
27. Theodorakakos A, Strotos G, Mitroglou N, Atkin C, Gavaises M. Friction-induced heating in nozzle hole micro-channels under extreme fuel pressurisation. *Fuel*. 2014;123(x):143-150.
28. Strotos G, Koukouvinis P, Theodorakakos A, Gavaises M, Bergeles G. Transient heating effects in high pressure Diesel injector nozzles. *Int J Heat Fluid Flow*. 2015;51:257-267.
29. Shi J, Guerrassi N, Dober G, Karimi K, Meslem Y. Complex physics modelling of diesel injector nozzle flow and spray supported by new experiments. *THIESEL 2014 Conf. Thermo-Fluid Dynamics. Process Direct Inject Engines*. 2014.
30. Shi J, Aguado PL, Dober G, Guerrassi N, Bauer W, Lai M. Using LES and x-ray imaging to understand the influence of injection hole geometry on Diesel spray formation. *THIESEL 2016 Conf. Thermo-Fluid Dynamics Process Diesel Engines Conference Thermo Fluid Dynamics*. 2016.
31. Shi J, Aguado Lopez P, Gomez Santos E, Guerrassi N, Dober G, Bauer W, Lai M, Wang J. Evidence of vortex driven primary breakup in high pressure fuel injection. *Proc. ILASS–Europe 2017 28th Conf. on Liquid Atomization and Spray System* (ILASS), Valencia, Spain, 2017.
32. Shi J, Lopez PA, Santos EG, et al. High Pressure Diesel Spray development : the effect of nozzle geometry and flow vortex dynamics. *14th Triennial International Conf. on Liquid Atomization and Spray Systems (ICLASS)*, Chicago, IL, USA, 2018.
33. Strotos G, Gavaises M, Theodorakakos A, Bergeles G. Evaporation of a Suspended Multicomponent Droplet Under Convective Conditions. *Proc. of CHT-08 International Symposium on Adavances in Computational Heat Transfer* (ICHMT), Marrakech, Morocco, 2008.
34. Stefanitsis D, Malgarinos I, Strotos G, Nikolopoulos N, Kakaras E, Gavaises M. Numerical investigation of the aerodynamic breakup of Diesel and heavy fuel oil droplets. *Int J Heat Fluid Flow*.2017;68:203-215.
35. Papoutsakis A, Theodorakakos A, Giannadakis E, Papoulias D, Gavaises M. LES Predictions of the Vortical Flow Structures in Diesel Injector Nozzles. *SAE Tech Pap 2009-01-0833*, 2009.
36. Yuan W, Schnerr GH. Numerical Simulation of Two-Phase Flow in Injection Nozzles: Interaction of Cavitation and External Jet Formation. *J Fluids Eng*. 2004;125(6):963-969.
37. Lauer E, Hu XY, Hickel S, Adams NA. Numerical investigation of collapsing cavity arrays. *Phys Fluids*. 2012;24(5):52104.
38. Kubota A, Kato H, Yamaguchi H. Finite difference analysis of unsteady cavitation on a two-dimensional hydrofoil. *Fifth International Conference on Numerical Ship Hydrodynamics* (ICNSH), Hiroshima, Japan, 1990.

39. Kunz RF, Boger D a, Stinebring DR, et al. A preconditioned Navier - Stokes method for two-phase flows with application to cavitation prediction. *Comput Fluids*. 2000;29:849-875.
40. Schnerr GH, Sauer J. Physical and Numerical Modeling of Unsteady Cavitation Dynamics. *Fourth International Conference on Multiphase Flow* (ICMF), New Orleans, USA, 2001.
41. Zwart PJ, Gerber AG, Belamri T. A Two-Phase Flow Model for Predicting Cavitation Dynamics. *Fifth International Conference on Multiphase Flow* (ICMF), Yokohama, Japan, 2004.
42. Goel T, Thakur S, Haftka R, Shyy W, Zhao J. Surrogate Model-Based Strategy for Cryogenic Cavitation Model Validation and Sensitivity Evaluation. *42nd AIAA/ASME/SAE/ASEE Joint Propulsion Conference & Exhibit*, Sacramento, California, USA, 2006.
43. Niedzwiedzka A, Schnerr GH, Sobieski W. Review of numerical models of cavitating flows with the use of the homogeneous approach. *Arch Thermodyn*. 2016;37(2):71-88.
44. Cristofaro M, Edelbauer W, Koukouvinis P, Gavaises M. A numerical study on the effect of cavitation erosion in a diesel injector. *Appl Math Model*. 2020;78:200-216.
45. Wang C, Moro A, Xue F, Wu X, Luo F. The influence of eccentric needle movement on internal flow and injection characteristics of a multi-hole diesel nozzle. *Int J Heat Mass Transf*. 2018;117:818-834.
46. Katz J, Cristofaro M, Edelbauer W, Koukouvinis P, Gavaises M. Large Eddy Simulation of the Internal Injector Flow During Pilot Injection. *Proc. 10th Int Symp Cavitation*. 2019:9-12.
47. Edelbauer W. Numerical simulation of cavitating injector flow and liquid spray break-up by combination of Eulerian–Eulerian and Volume-of-Fluid methods. *Comput Fluids*. 2017;144:19-33.
48. Moro A, Luo T, Wang C, Luo F. Eccentric needle displacement effect on spray formation from a multi orifice diesel injector. *Heat Mass Transf und Stoffuebertragung*. 2019.
49. Greif D, Edelbauer W, Strucl J. Numerical Simulation Study of Cavitating Nozzle Flow and Spray Propagation with Respect to Liquid Compressibility Effects. *SAE Tech Pap 2014-01-1421*, 2014.
50. Cristofaro M, Edelbauer W, Gavaises M, Koukouvinis P. Numerical simulation of compressible cavitating two-phase flows with a pressure-based solver. *Proc. ILASS–Europe 2017 28th Conf. on Liquid Atomization and Spray System* (ILASS), Valencia, Spain, 2017.
51. Cristofaro M, Edelbauer W, Koukouvinis P, Gavaises M. Influence of Diesel fuel viscosity on cavitating throttle flow simulations at erosive operation conditions. *ACS Omega*. 2020;5(13):7182-7192.
52. von Berg E, Edelbauer W, Alajbegovic A, et al. Coupled Simulations of Nozzle Flow, Primary Fuel Jet Breakup, and Spray Formation. *J Eng Gas Turbines Power*. 2005;127(4):897.

53. Waidmann W, Boemer A, Braun M. Adjustment and verification of model parameters for Diesel injection CFD simulation. *SAE Tech Pap*. 2006;2006(724).
54. Luo F, Cui H, Dong S. Transient measuring method for injection rate of each nozzle hole based on spray momentum flux. *Fuel*. 2014;125:20-29.
55. Luo T, Jiang S, Moro A, Wang C, Zhou L, Luo F. Measurement and validation of hole-to-hole fuel injection rate from a diesel injector. *Flow Meas Instrum*. 2018;61:66-78.
56. Zhou LY, Dong SF, Cui HF, Wu XW, Xue FY, Luo FQ. Measurements and analyses on the transient discharge coefficient of each nozzle hole of multi-hole diesel injector. *Sensors Actuators, A Phys*. 2016;244:198-205.
57. Yin B, Yu S, Jia H, Yu J. Numerical research of diesel spray and atomization coupled cavitation by Large Eddy Simulation (LES) under high injection pressure. *Int J Heat Fluid Flow*. 2016;59:1-9.